Journal of Power Sources 226 (2013) 346–353

Contents lists available at SciVerse ScienceDirect

Journal of Power Sources

journal homepage: www.elsevier.com/locate/jpowsour

Highly durable polymer electrolyte membranes at elevated temperature: Cross-linked copolymer structure consisting of poly(benzoxazine) and poly(benzimidazole)

Sung-Kon Kim [a], Ki-Hyun Kim [b], Jung Ock Park [b], Kihyun Kim [a], Taeyun Ko [a], Seong-Woo Choi [b], Chanho Pak [b], Hyuk Chang [b], Jong-Chan Lee [a,*]

[a] Department of Chemical and Biological Engineering, and Institute of Chemical Process, Seoul National University, 599 Gwanak-ro, Gwanak-gu, Seoul 151-744, Republic of Korea
[b] Energy Lab., Samsung Advanced Institute of Technology, Samsung Electronics Co., Ltd., Nongseo-dong, Giheung-gu, Gyeonggi-do, 446-712, Republic of Korea

HIGHLIGHTS

- Cross-linked copolymers were prepared by PBI and difunctional benzoxazine.
- Excellent thermal and mechanical stabilities of cross-linked copolymer membranes.
- Performance and durability of cross-linked copolymer membranes was highly enhanced.

GRAPHICAL ABSTRACT

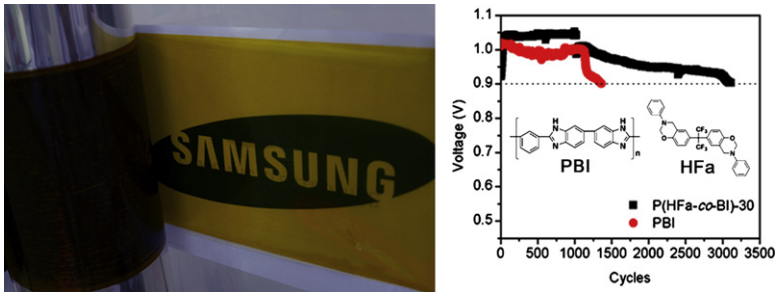

ARTICLE INFO

Article history:
Received 6 October 2012
Received in revised form
7 November 2012
Accepted 9 November 2012
Available online 19 November 2012

Keywords:
Fuel cells
Membranes
Poly(benzimidazole)
Poly(benzoxazine)
Phosphoric acid

ABSTRACT

For polymer electrolyte membrane fuel cell (PEMFC) applications at elevated temperature (>100 °C), a series of cross-linked benzoxazine–benzimidazole copolymer, P(HFa-*co*-BI), membranes are prepared by casting a solution of poly[2,2′-(*m*-phenylene)-5,5′-bibenzimidazole] (PBI) and di-functional benzoxazine monomer, 6,6′-(hexafluoroisopropylidene)bis(3-phenyl-3,4-dihydro-2*H*-benzoxazine) (HFa), in *N*,*N*-dimethylacetamide prior to stepwise heating to 250 °C. The films are also viable to manufacture to large quantities and area by roll-to-roll coating. The resulting cross-linked copolymer, P(HFa-*co*-BI), membranes are found to be thermally and mechanically stable. Although the proton conductivity values of P(HFa-*co*-BI) membranes are smaller than that of the PBI membrane, their cell performance (0.68 V at 0.2 A cm^{-2} at 150 °C) is close to that of PBI membrane and their long-term durability (*ca.* 3116 cycles on *in situ* accelerated lifetime mode of load cycling testing) is found to be far superior to the PBI membrane.

1. Introduction

In recent years, considerable attention has been paid to the development of polymer electrolyte membrane fuel cells (PEMFCs) at elevated temperature (>100 °C) and low humidity (relative humidity < 50%) conditions [1,2]. Compared with PEMFCs at low temperature, those at elevated temperature may potentially offer numerous advantages, including (1) rapid electrode kinetics, (2) no need for water management, (3) a higher tolerance to significant quantities of carbon monoxide, (4) no cathode flooding by the water produced, and (5) a simplified system design [3–7]. Phosphoric acid (PA)-doped poly(benzimidazole) membranes have gained enormous attention as one of the most promising candidates as PEMs in the

* Corresponding author. Tel.: +82 2 880 7070; fax: +82 2 880 8899.
E-mail address: jongchan@snu.ac.kr (J.-C. Lee).

0378-7753/$ – see front matter © 2012 Elsevier B.V. All rights reserved.
http://dx.doi.org/10.1016/j.jpowsour.2012.11.019

elevated temperature fuel cell processes. Poly[2,2′-(*m*-phenylene)-5,5′-bibenzimidazole] (PBI) has especially been most widely used as a membrane material [8–14]. Since PA itself has a larger proton conductivity value and reasonably good thermal stability at elevated temperatures, the poly(benzimidazole) membranes prepared by doping procedure in PA solution have good proton transport capability and thermal stability for use in fuel cells at elevated temperatures. For example, high proton conductivity values, even larger than 0.1 S cm^{-1}, of PA-doped poly(benzimidazole) membranes have been substantiated by several studies [8,9,12,13]. In many cases, a large amount of PA in the membranes is needed to achieve the desired proton conductivity. Excess amount of PA in the membranes, however, results in the dissolution of poly(benzimidazole)s, which could limit the practical application of poly(benzimidazole) membranes for PEMs [9]. To date, many attempts have been made to improve the stability of poly(benzimidazole) membranes in PA using cross-linking [15], blending [16], copolymerization [17], and hybrids with inorganic materials [18]. However, there are only few reports, if any, on poly(benzimidazole) membranes showing both good fuel cell performance and long-term durability. The long-term durability is particularly one of the most important issues for practical applications of the membrane materials for fuel cells. We recently prepared cross-linked copolymeric membranes by mixing PBI or poly(2,5-benzimidazole) with mono-functional benzoxazines such as 3-phenyl-3,4-dihydro-6-*tert*-butyl-2*H*-1,3-benzoxazine and 6-fluoro-3-(pyridin-2-yl)-3,4-dihydro-2*H*-benzoxazine, followed by stepwise heating for the formation of cross-linked copolymeric structures [19,20]. Although these membranes doped with PA showed quite large proton conductivity and very good fuel cell performance, their long-term stability need to be improved for practical applications; their stable cycle life obtained from load cycling testing using *in situ* accelerated lifetime mode was less than 2000 cycles. It is well-known that a series of poly(benzoxazine) derivatives having different physical and chemical properties could be prepared because versatile molecular design of benzoxazine monomers is possible by changing the functional groups attached to the benzoxazine framework and the number of benzoxazine ring groups. Also, the cross-linked structure and highly fluorinated functional groups provide improved physical properties for the polymer membranes [15].

This time we found that membrane-electrode assemblies (MEAs) using PA-doped cross-linked copolymer (referred to here as P(HFa-*co*-BI)) membranes composed of PBI and a highly fluorinated di-functional benzoxazine, 6,6′-(hexafluoroisopropylidene)bis(3-phenyl-3,4-dihydro-2*H*-benzoxazine), show very excellent long-term stability (stable cycle life for 3116 cycles obtained from load cycling testing using *in situ* accelerated lifetime mode) with reasonably good fuel cell performance (0.68 V at 0.2 A cm^{-2}). Although the proton conductivities of PA-doped P(HFa-*co*-BI) membranes (<0.05 S cm^{-1} at 150 °C) are smaller than that of PA-doped PBI membrane (~0.07 S cm^{-1} at 150 °C), they show very similar fuel cell performance. The long-term stability of P(HFa-*co*-BI) membranes is much better than that of the PBI membrane and previous cross-linked copolymer membranes from the mono-functional benzoxazines. The intriguing properties of a series of membranes and MEAs such as thermooxidative, chemical, mechanical stabilities, proton conductivity, and fuel cell performance are fully discussed in this paper. Furthermore, the correlation of benzoxazine content and cell performance is comprehensively investigated by electrochemical analyses.

2. Experimental

2.1. Materials

Isophthalic acid (99%) was purchased from Aldrich and purified by recrystallization in ethanol to obtain white needle-like products. 3,3′-Diaminobenzidine (97%, Tokyo Kasei, TCI), poly(phosphoric acid) (PPA, 116% H_3PO_4, Junsei), phosphorous pentoxide (97%, Aldrich), phosphoric acid (PA, 85 wt.% aqueous solution, Aldrich), toluene (99.8%, Aldrich), poly(vinylidene fluoride) (PVDF, Mn ~107,000 g mol^{-1}, Mw ~275,000 g mol^{-1}, Aldrich), *p*-formaldehyde (95%, Aldrich), 4,4′-(hexafluoroisopropylidene)diphenol (97%, Aldrich), bisphenol A (97%, Aldrich), and aniline (99%, Aldrich) were used without further purification. Other solvents were used as received.

2.2. Synthesis of 6,6′-(hexafluoroisopropylidene)bis(3-phenyl-3,4-dihydro-2H-benzoxazine) (HFa)

Stoichiometric amounts of 4,4′-(hexafluoroisopropylidene) diphenol (10.0 g, 29.7 mmol), *p*-formaldehyde (4.13 g, 130 mmol), and aniline (6.15 g, 65.4 mmol) were used in the corresponding benzoxazine monomer synthesis. In a 250 mL two neck round-bottomed flask equipped with condenser and nitrogen inlet, *p*-formaldehyde and aniline were added in 100 mL toluene and mixed at 110 °C for 1 h until the solution became transparent. 4,4′-(Hexafluoroisopropylidene)diphenol was added to the mixture and refluxed for 4 h. The reaction mixture was washed twice with 1 N NaOH aqueous solution (200 mL) and rinsed several times with distilled water and then dried with anhydrous magnesium sulfate. Removal of solvent by evaporation and drying under vacuum afforded HFa as white powder. Yield: >95%. Anal Cald: C, 65.2; H, 4.24; N, 4.91. Found: C, 65.2; H, 4.20; N, 4.91. ^{1}H NMR (500 MHz, DMSO-d_6, ppm): δ 7.24 (t, J = 7.75 Hz, 4H), 7.13 (m, 6H), 7.00 (d, J = 8.50 Hz, 2H), 6.87 (t, J = 8.50, 2H), 6.82 (d, J = 8.50, 2H), 5.51 (s, 4H), 4.68 (s, 4H). ^{13}C NMR (125 MHz, DMSO-d_6, ppm): δ 154.0, 146.9, 128.6, 127.8, 123.4, 120.9, 116.6, 115.8, 78.30, 48.29.

2.3. Preparation of P(HFa-co-BI) membranes

Poly[2,2′-(*m*-phenylene)-5,5′-bibenzimidazole] (PBI) was synthesized as reported previously (Fig. 1) [19]. P(HFa-*co*-BI)s were prepared by reacting different weight% of HFa to PBI. When the weight% of HFa was 40, 30, 20, and 10, they are represented by P(HFa-*co*-BI)-40, P(HFa-*co*-BI)-30, P(HFa-*co*-BI)-20, and P(HFa-*co*-BI)-10, respectively. The polymer films were prepared using typical solution casting techniques prior to subsequent stepwise heating as described in detail in Supplementary data. The thickness of the dried films ranged from 30 to 50 μm. For achieving the proton conduction ability of the membrane, the dried films were immersed in 1000 mL of the PA solution with 80–85 wt.% concentration at 80 °C for 4 h. The PA-doped membranes were taken out from the PA solution and then blotted with filter paper. The PA-doped membranes were dried at 70 °C under vacuum for 2 days and weighed again (W_{doped}). The PA within the membranes was intentionally removed by rinsing with an aqueous solution of $NaHCO_3$ and distilled water several times in order to measure the PA content. The films were then dried for 2 days in a vacuum oven and weighed ($W_{undoped}$). The weight difference, ($W_{doped} - W_{undoped}$), was assumed to be the weight of the absorbed PA. The PA content of the membrane was then calculated as the weight percent (wt.%) of PA absorbed in the membrane using Eq. (1).

$$\text{PA content(wt.\%)} = \left(W_{doped} - W_{undoped}\right) \Big/ W_{doped} \times 100 \quad (1)$$

The PA-doped PBI membranes were also prepared by solution casting method commonly used [21].

For large-sized scale film production (25 cm × 880 m), the mixed solution of HFa and PBI in DMAc was prepared as a concentrated solution (30 wt.%). The films were coated on poly(ethylene terephthalate) (PET) base film and produced continuously using a slot die coater with a total length of 35 m and floating dryers.

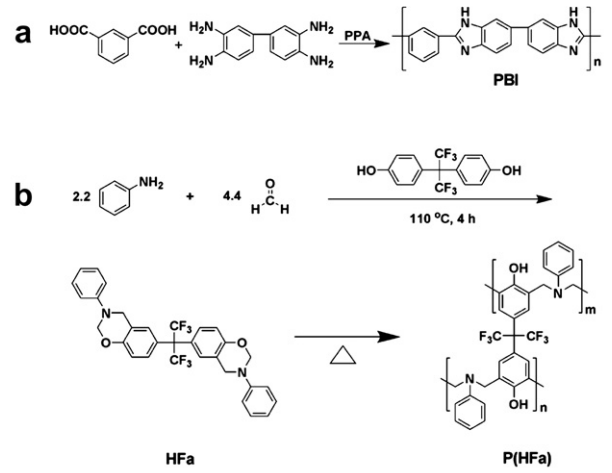

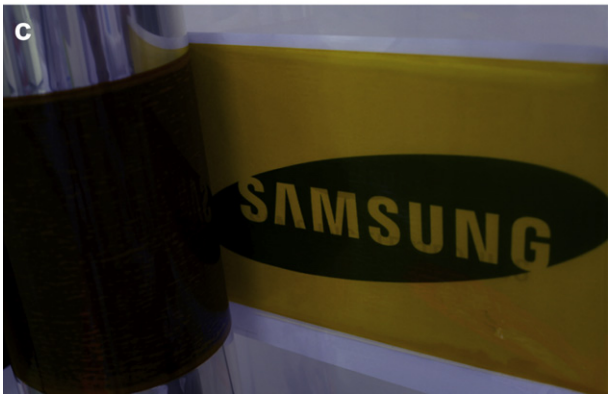

Fig. 1. Synthesis of a) PBI, b) HFa and P(HFa), c) large scale (25 cm × 880 m) P(HFa-*co*-BI) film by roll-to-roll coating.

Drying zones were divided into nine compartments with a total length of 27 m from 80 to 120 °C. The machine speed was 2 m min^{-1}. The coated and dried films were detached from PET base film and then transferred to an oven, followed by stepwise thermal treatment from 100 to 250 °C for 5 h.

2.4. Preparation of membrane-electrode assembly (MEA)

The slurry for forming catalyst layer was prepared by adding catalyst powder into PVDF solution in *N*-methyl-2-pyrrolidone (NMP). After the slurry was spread on the wet-proofed carbon evenly by automated doctor blade technique, the electrode catalyst layer was dried at 120 °C for 2 h under a ventilated oven. Each electrode catalyst layer was consisted of PtCo alloy supported on carbon (Tanaka Kikinzoku Kogyo K.K., TEC36E52) and PVDF on the cathode, and PtRu supported on carbon (Tanaka Kikinzoku Kogyo K.K., TEC61E54) and PVDF on the anode, respectively. The mean platinum loading was 0.9 mg cm^{-2} on the anode and 1.7 mg cm^{-2} on the cathode. The PA-doped membrane was mounted into a single cell, and then the electrodes and membrane without a preceding hot-pressing step were assembled in a homemade single cell with graphite bipolar plates and gold-plated copper end plates, the active area in MEA was about 7.84 cm^2; the assembling torque was 3 N m.

2.5. Characterization

The ^1H and ^{13}C nuclear magnetic resonance (NMR) spectra were collected on a Bruker Avance 500 with a proton frequency of 500 MHz. During the experiments, deuterated dimethylsulfoxide (DMSO-d_6) was used as the solvent and tetramethylsilane (TMS) was used as the internal standard. Gel fractions were measured by solvent extraction [22]. The films, 2 cm × 2 cm in size, were dried at 70 °C under vacuum for 2 days and weighed (W_1), and then the dried films were soaked in an excess of 85 wt.% PA solution at 160 °C for 24 h. The films after extraction were washed with distilled water several times. The films were dried for 2 days in a vacuum oven until constant weight and reweighed (W_2). The gel fractions were calculated as follows:

$$\text{Gel fraction (\%)} = W_2/W_1 \times 100 \quad (2)$$

The P(HFa) units per PBI repeat unit were estimated by the weight change upon PA doping. 2 cm × 2 cm films were dried at 70 °C under vacuum for 2 days, weighed (W_3), and immersed in 85 wt.% PA solution at 80 °C for 4 h. They were then repeatedly washed with distilled water and dried for 2 days in a vacuum oven until constant weight (W_4). P(HFa) units per PBI repeat unit were calculated as follows:

$$P(\text{HFa}) \text{ units per PBI repeat unit} = \{[W_3 \times \text{HFa content}/100 - (W_3 - W_4)]/\text{MW}_{\text{HFa}}\} / [W_3 \times \text{PBI content}/100 / \text{MW}_{\text{PBI}}] \quad (3)$$

where HFa content and PBI content are their weight% in the membrane and MW_{HFa} and MW_{PBI} are the molecular weights of the HFa (570.52 g mol^{-1}) and the PBI (308.34 g mol^{-1}) repeat units, respectively. The mechanical properties were measured using a universal testing machine (Lloyd LR-10K). The dumbbell specimens were prepared using the ASTM standard D638 (Type V specimens dog-bone shaped samples). The tensile properties of the PA-doped membrane samples were measured in air at 23 °C under a 45% relative humidity (RH) with a gauge length and cross head speed of 15 mm and 10 mm min^{-1}, respectively. The proton conductivity of membranes was measured using *ex situ* electrochemical impedance spectroscopy (EIS) technique fitted with a four probe. The impedance measurements were carried out using a ZAHNER IM-6ex impedance analyzer in potentiostat mode with a perturbation amplitude of 10 mV over the frequency range, 1 Hz to 1 MHz. The impedance at a controlled humidity and temperature was measured from a Nyquist plot. For the Nyquist plot, both the real (Z′) and imaginary parts (Z″) of the components of impedance in the membrane sample were measured simultaneously over the defined frequency range. The real Z′-axis intercept was close to the ohmic resistance (R) of a membrane sample. The proton conductivity (σ) was calculated using the equation, $\sigma = d/RS$, where d is the distance between the reference and sensing electrodes, and S is the cross-section area (thickness × width) of a doped membrane. The membranes, 1 cm × 5 cm in size, were introduced to the conductivity cell and heated to 160 °C. The cell was maintained at this temperature for 30 min, and the measurements were taken while cooling the cell to 100 °C in 10 °C steps. The *in situ* EIS of single cells were measured using an impedance/gain-phase analyzer (Solartron SI1260) after fully activating them. The dried hydrogen gas at 25 °C was fed onto both anode and cathode compartments for a total of 2 h 30 min, and then the temperature of single cells was raised up to 150 °C. The flow rate of hydrogen gas was controlled to 150 sccm during the measurements. As soon as the temperature was reached to 150 °C, the frequency was swept in a frequency range of 10^5 to 1 Hz with an amplitude of 10 mV at 150 °C. The cell performance and *in situ* acceleration lifetime test (ALT) were executed on a home-made fuel cell test station. The unit cell was operated at 150 °C with hydrogen as a fuel and air without

humidification at ambient pressure and a flow rate of 100 and 250 cc min^{-1}, respectively. In case of *in situ* ALT, the cell voltage was altered continuously through the stepwise load circulation and recorded in its steady state at each load without fluctuation. The current density was increased stepwise from zero to 1.0 A cm^{-2} for 1 h, and then recurred to zero again. Such cycling was repeated until open circuit voltage (OCV) dropped below 0.9 V.

3. Results and discussion

Fig. 1 shows the chemical reactions for the formation of poly [2,2′-(*m*-phenylene)-5,5′-bibenzimidazole] (PBI, inherent viscosity: 0.85 dL g^{-1}) and 6,6′-(hexafluoroisopropylidene)bis(3-phenyl-3,4-dihydro-2*H*-benzoxazine) (HFa), and the polymerization of HFa to P(HFa) that could be simply obtained by heating the HFa at 250 °C for 1 h. The detailed synthesis and chemical characterization of the P(HFa-*co*-BI)s are in the Supplementary data (Fig. S1).

Previously we prepared PA-doped cross-linked copolymer membranes for applications in polymer electrolyte membrane fuel cells (PEMFCs) at elevated temperature [19,20]. These copolymers were prepared from mono-functional benzoxazines (having one benzoxazine ring group) with poly(benzimidazole)s. The formation of the covalent bonding between the benzoxazine and benzimidazole units producing cross-linked copolymeric structures was confirmed by spectroscopy and chemical stability studies. The ring-opening of benzoxazine monomer by thermal treatment occurs; its polymerization can proceed spontaneously by adding another benzoxazine monomer. At this time, the benzoxazine monomer can also be reacted with poly(benzimidazole)s covalently, resulting in cross-linked copolymeric structures. It is well-known that a series of poly(benzoxazine) derivatives having different physical and chemical properties could be prepared because versatile molecular design of benzoxazine monomers is possible by changing the functional groups attached to the benzoxazine framework and the number of benzoxazine ring groups. In this study, cross-linked copolymer membranes were prepared from the di-functional benzoxazine monomer (having two benzoxazine ring groups), HFa, with PBI using the solution casting method followed by subsequent stepwise heating. This procedure is in line with those for the preparation of cross-linked copolymer membranes from mono-functional benzoxazines, except for the heating temperature [19,20]. It is known that benzoxazine monomers with different chemical structures have different ring opening polymerization temperatures [23]. The formation of the covalently cross-linked copolymer structure of the products is discussed in detail in the Supplementary data (Fig. S2). The name of the resulting cross-linked copolymers were abbreviated as P(HFa-*co*-BI)-X, where X represents the HFa to PBI weight%. When the composition of HFa to PBI is over 40 wt.%, the resulting films became opaque and brittle, yielding their premature failure.

In Fig. 1c, P(HFa-*co*-BI) films were scalable to 25 cm × 880 m in size using a conventional slot die coating machine through the continuous process [19,24]. The large-sized films could be produced simply by mixing of PBI solution with HFa monomer and then were coated on poly(ethylene terephthalate) (PET) base film. After drying, the films were peeled off from the PET base film and we thus obtained free-standing films composed of PBI and HFa monomer. The cross-linked copolymer membranes were then produced by stepwise heating from 100 to 250 °C for 5 h in an oven. We confirmed that the cell performance and durability of large-sized films prepared were found to be almost identical with those of small-sized films (20 cm × 30 cm).

The thermal and thermooxidative stability of the undoped polymers was examined by thermogravimetric analysis (TGA) under an air atmosphere, and their degradation temperatures were obtained by heating the samples up to 800 °C. All P(HFa-*co*-BI) samples are thermally stable up to 420 °C (Fig. S3 in Supplementary data). The decomposition temperatures of P(HFa), P(HFa-*co*-BI)-40, -30, -20, -10, and PBI, at which they retained 90% of their initial weight, are 432, 444, 440, 426, 423, and 302 °C, respectively. PBI shows a small weight loss from the evaporation of absorbed water at around 100 °C [9]; its weight is then maintained up to 500 °C, demonstrating excellent thermal and thermooxidative stability. As HFa units are less hygroscopic than the imidazole units in PBI, P(HFa-*co*-BI)s show smaller initial water loss at around 100 °C, the boiling point of water. Interestingly, the decomposition temperatures of P(HFa-*co*-BI)s increase with increasing HFa content because of the higher decomposition temperature of P(HFa). The thermal behavior results clearly indicate that the P(HFa-*co*-BI)s are thermally stable within the temperature range of PEMFC applications.

PA contents obtained by the immersion of the membranes in 80 or 85 wt.% PA baths are presented in Fig. 2. The increase of PA content with increasing PA concentration is typical for PA-doped PBI membranes. All of the P(HFa-*co*-BI) membranes show smaller PA content than the PBI membrane, and their PA contents decrease with increasing HFa content when the same PA bath was used. Since the P(HFa-*co*-BI) membranes with larger HFa content have larger gel fraction (or degree of cross-linking) and larger content of hydrophobic fluorinated hexafluoroisopropylidene groups, they should absorb less amount of hydrophilic and polar PA [25]. It is well-known that membranes having cross-linked structure absorb less amount of PA than those prepared from linear polymers [15]. TGA results (Fig. S3 in Supplementary data) also clearly indicate that P(HFa-*co*-BI)s having larger content of HFa absorb less amount of polar water; they show smaller water loss at around 100 °C. The lower basicity of *tert*-amine groups in HFa units compared to the imidazole units in PBI can also be attributed to the smaller PA content of the P(HFa-*co*-BI) having larger content of HFa units [9,20].

The proton conductivities of the P(HFa-*co*-BI) membranes with different PA content were evaluated using *ex situ* electrochemical impedance spectroscopy (EIS) at 100–160 °C under anhydrous conditions (Fig. S4). The proton conductivity versus temperature curves exhibit Arrhenius behavior ($\sigma = \sigma_0 \exp(-E_a/RT)$, where σ_0 is the pre-exponential factor and E_a is the activation energy for the proton conduction). Therefore the introduction of HFa into the membrane structure does not change the mechanism of proton transport behavior, if any. The proton transport follows the proton-hopping dominant mechanism (Grotthuss-type mechanism) as

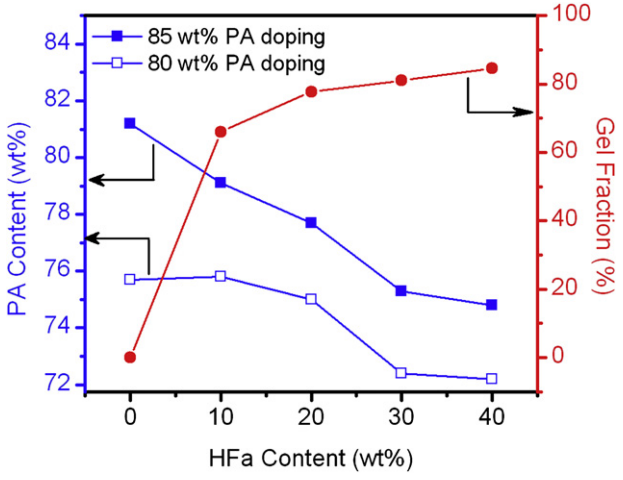

Fig. 2. PA contents and gel fraction of P(HFa-*co*-BI)s as a function of HFa content.

reported by others [26,27]. Fig. 3a represents the proton conductivities of PA-doped membranes at 120 and 150 °C under anhydrous conditions after being doped in 80 or 85 wt.% PA baths. All P(HFa-*co*-BI) membranes show smaller proton conductivity values than the PBI membrane, and their proton conductivities decrease with increasing HFa content although proton conductivities decrease much less or show a plateau when P(HFa-*co*-BI)s have HFa content larger than 20 wt.%. The changes in proton conductivity with HFa content could be correlated to the gel fraction (or degree of cross-linking), PA content, and the contents of benzoxazine units in the membrane. The increase of the cross-linked structures in the membranes can decrease the proton conductivity, because they can restrict polymer chain mobility [22], while the increase of the HFa content can increase or decrease the proton conductivity. Since HFa is quite hydrophobic, the increase of the HFa units in the structure can decrease the absorption of PA, which results in decreased proton conductivity. It was found in our previous studies, however, that the increase of the benzoxazine units in the membrane structures can increase the proton conductivity; the benzoxazine units can impart additional hopping sites for proton and the increase of chain length of benzoxazine units can increase the free volume in the membrane [19,20]. These combined effects should produce proton conductivity behavior with the changes of HFa units in Fig. 3b. For example, the inclusion of 10 wt.% of HFa decreases the proton conductivity for a large degree because the addition of a small amount of hydrophobic HFa in the membrane results in quite compact cross-linked structures giving very small free volumes in the membrane structure. When the content of HFa increases further, the conductivity decreases due to the decrease of the PA content, while the extent of decrease is less pronounced due to the increase of the free volume and the hopping sites.

Fig. 4 shows current–voltage (*I–V*) curves of the cells that used MEAs with PA-doped membranes at 150 °C with hydrogen/air gas without humidification at ambient pressure. The thickness and PA content of all membranes were kept at the same level of approximately 60 μm and 75 wt.%, respectively. Fig. 4 displays that the voltage of cells increases with the increase in HFa content in the P(HFa-*co*-BI) membranes. In general, membranes having larger proton conductivity values have larger cell performance values than those having smaller proton conductivity values [9]. Still, the voltage of cells with the P(HFa-*co*-BI)-30 and P(HFa-*co*-BI)-40 membranes are fairly comparable to that with PBI membrane over the entire range of current density, although their proton conductivity values are smaller than that of the PBI membrane (Fig. 3).

Since the same electrodes were used for the measurements, the cell performance behavior could be attributed to membrane-associated properties such as membrane resistance and interfacial resistance at the membrane/electrodes interface [28]. It was reported that the interface resistance between membrane and electrodes are affected by the fluorine concentration at the membrane–electrode interface of MEAs fabricated using Nafion as both the binder and membrane materials [28–30]. The elemental composition and concentration of the membrane surface were analyzed by field-emission scanning microscopy coupled with energy dispersive spectroscopy (FE-SEM/EDS, Fig. S5). The EDS spectrum of PBI clearly shows the presence of carbon, oxygen, and nitrogen, whereas that of P(HFa-*co*-BI)s reveals the additional presence of fluorine as expected. The fluorine concentration of P(HFa-*co*-BI)s increases with increasing HFa content, and the atomic percentages of fluorine for P(HFa-*co*-BI)-40,-30,-20, and -10 are 8.80, 6.31, 4.39, and 3.64, respectively. As the highly fluorinated polymer, PVDF, was used as a binder in the electrodes, the compatibility between the membrane and electrodes seems to be enhanced by increasing the content of HFa units containing fluorine

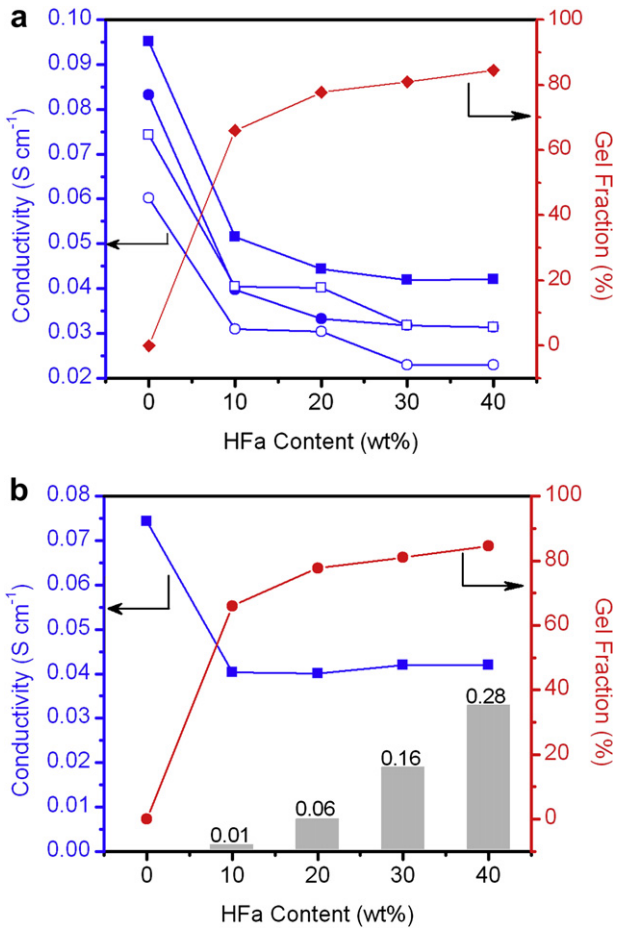

Fig. 3. a) At 120 °C (open symbols) and 150 °C (closed symbols) under anhydrous conditions, proton conductivity of P(HFa-*co*-BI) membranes as a function of HFa content after immersion in 80 wt.% (circle) or 85 wt.% (square). b) Proton conductivity for a 75 wt.% of PA-doped P(HFa-*co*-BI) membranes at 150 °C under anhydrous conditions. Columns in figure denote P(HFa) units per PBI repeat unit, determined according to the Eq. (3).

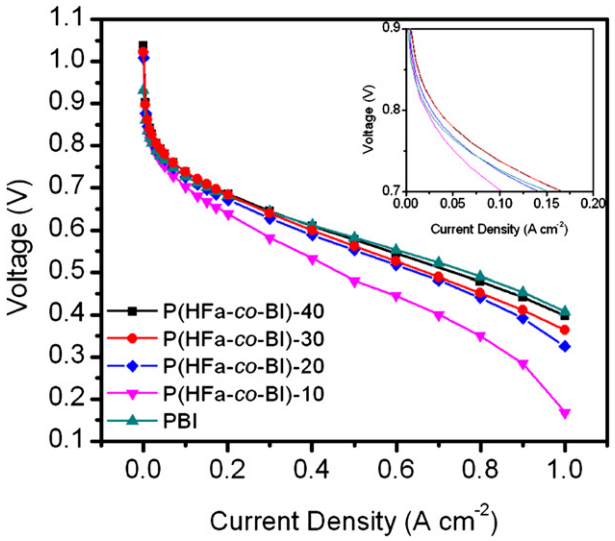

Fig. 4. Current–voltage (*I–V*) curves of PA-doped P(HFa-*co*-BI) membranes at 75 wt.% PA content at 150 °C, non-humidified H_2 and air (ambient pressure), cathode; 0.9 mg cm^{-2} PtRu loading, anode; 1.7 mg cm^{-2} PtCo loading. Active area is 7.84 cm^2. (Inset) the enlargement of polarization curves in the range of 0.0–0.2 A cm^{-2}.

moiety. The high concentration of fluorine on the surface of the membrane appears to improve its compatibility with the electrode surface and decreases contact resistance between the membrane and electrode and this could increase the cell performance of the P(HFa-*co*-BI) membranes. Accordingly, the increased compatibility between the P(HFa-*co*-BI) membrane and electrode interface could originate from the fluorinated groups of HFa units.

In order to understand the cell performance results of the P(HFa-*co*-BI) and PBI membranes, an electrochemical analysis of the cells was performed using a cyclic voltammogram (CV, Fig. S6) and *in situ* EIS in the symmetrical mode (Fig. 5). The measurements were conducted on cells with the P(HFa-*co*-BI)-40 membrane having the largest fluorine content and a PBI membrane with no fluorine groups. The electrochemical surface areas (ESAs) of the electrodes assembled with the P(HFa-*co*-BI)-40 and PBI membranes were almost identical at about 14.6 $m^2\ g^{-1}$. The ESAs of the electrodes in the cell with the P(HFa-*co*-BI)-10 to -30 membranes were also tested, and found to be somewhat different from those of PBI and P(HFa-*co*-BI)-40 membranes. Thus, the *in situ* EIS results of P(HFa-*co*-BI)-10 to -30 cannot be directly compared to those of P(HFa-*co*-BI)-40 and PBI, because the electrochemical behaviors in the MEAs depend on the extent of ESAs. Fig. 5 shows the impedance spectra of the two cells that were evaluated at OCV with an H_2 feed in both the anode and cathode sides at 150 °C under unhumidified conditions. EIS has been commonly evaluated in the normal mode of PEMFCs with H_2/O_2 (or air) gas-feeding. But, it is very difficult to distinguish the individual behaviors of the compartments such as the membrane, anode, and cathode, respectively. These drawbacks could be overcome by the use of the symmetrical mode, in which identical gas (H_2/H_2 gas-feeding in this study) was fed onto the anode and cathode compartments. This would allow the contribution of each compartment could be evaluated [31,32]. Given the schematic below, the advantages of the EIS measurement of the cell with an H_2/H_2 gas-feed over those with an H_2/O_2 gas-feed are i) the reduction in mass transfer resistance occurring in the presence of O_2 as a reactant gas, ii) no reaction product such as water, and iii) less heat production, making the cell an isothermal system [33].

(anode) $H_2 \rightarrow 2H^+ + 2e^-$

(cathode) $2H^+ + 2e^- \rightarrow H_2$

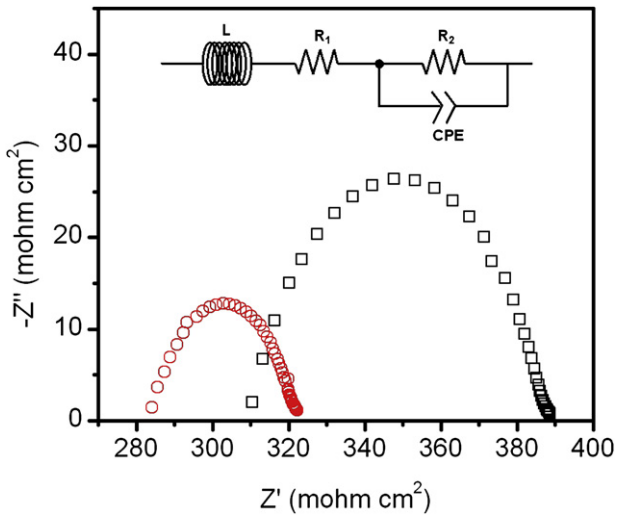

Fig. 5. Nyquist plots for cells employing (circle) P(HFa-*co*-BI)-40 and (square) PBI membranes in symmetrical mode with H_2/H_2 at 150 °C and non-humidified conditions. PA contents of the membranes were fixed to *ca.* 75 wt.%. The measurements were performed at OCV. (Inset) equivalent circuit fitted for the MEAs used in this study.

The left intercept of the semi-circle shown in Fig. 5 represents the membrane area resistance (R_m) of the cells, and it includes the membrane resistance, contact resistance, and minor ohmic losses of the electrodes [32]. Although the proton conductivity of P(HFa-*co*-BI)-40 is much smaller (by more than 50%) than that of the PBI membrane as confirmed by *ex situ* EIS in Fig. 3 at 150 °C under non-humidification conditions, the R_m value, 283 mΩ cm^2, measured from *in situ* EIS of the cell with the P(HFa-*co*-BI)-40 membrane is smaller than that, 310 mΩ cm^2, of the cell with a PBI membrane (Fig. 5). This result combined with the EDS result reflects that the high fluorine concentration on the membrane surface appears to improve its compatibility with the electrode surface and decreases contact resistance between the membrane and electrode.

In addition, the R_{ct} measured by the size of the radius of the semi-circle is determined by electrochemical reactions such as interface reaction kinetics, ionic conductivity, and diffusion limitations within the catalyst layer. The R_{ct} value, 39.0 mΩ cm^2, of the cells with the P(HFa-*co*-BI)-40 membrane, is also smaller than that, 79.0 mΩ cm^2, of the cell with the PBI membrane (Fig. 5). The smaller R_{ct} value measured from the P(HFa-*co*-BI)-40 membrane than that of the PBI membrane indicates the increase in electrochemical reaction rate at the membrane–electrodes interface. This finding was corroborated by the *I*–*V* results shown in Fig. 4, which show higher voltage for the cells with the P(HFa-*co*-BI)-20, -30, and -40 membranes than that of the cell with the PBI membrane in the kinetically controlled current density region (current density < 0.1 A cm^{-2}) [34]. In this region, the compatibility at the membrane/electrode interface can also influence the higher voltages of the cells with the P(HFa-*co*-BI) membrane, resulting in facilitated charge transfer [32,35]. Additionally, the presence of the fluorinated moieties in polymer structure increase the solubility of the gases such as H_2 and O_2 (the reactants on the electrode surface) and this can increase the electrochemical reaction rate in the electrode [36–39]. Consequently, the decrease in R_{ct} of the cell with the P(HFa-*co*-BI)-40 membrane relative to that of the PBI membrane can be ascribed to the increase in kinetic activity owing to the increase in gas concentration and the compatibility at the fluorinated membrane/electrodes interface.

The tensile strength, modulus, and elongation upon breakage of the PA-doped membranes were measured to estimate their mechanical properties (Table S1 and Fig. 6). Tensile strength and the modulus values decreased with increasing PA content in the membranes, whereas elongation at break increases. The tensile strength and modulus of P(HFa-*co*-BI) membranes initially increased with increasing HFa content, reach their maximum at a 20 wt.% of HFa content and then decreased as HFa content further increased to 40 wt.%. Previous studies reported that the tensile strength values of the membranes prepared from mono-functional benzoxazines were close or somewhat smaller than that of the PBI membrane [19,20]. On the other hand, the membranes prepared from di-functional benzoxazines, P(HFa-*co*-BI)s, exhibit remarkably increased tensile strength values compared to that of PBI membranes when HFa content is less than 10 wt.% (Fig. 6b). It is well-known that the high molecular weight of the polymers gives better mechanical strength to the membrane [40]. As the thermal dissociation of the mono-functional benzoxazines is accompanied by chain propagation during ring-opening polymerization, the linear poly(benzoxazine)s have been well-proven to have relatively low molecular weights [41,42]. Although the molecular weight of di-functional benzoxazines could not be obtained due to their extremely poor solubility in any solvent or strong acids, we believe that poly(benzoxazine)s starting from di-functional benzoxazines should have a larger amount of cross-linking and higher molecular weights than poly(benzoxazine)s prepared from the mono-functional benzoxazines. In particular, the P(HFa-*co*-BI)-20 and P(HFa-*co*-BI)-30 membranes show good mechanical stability for

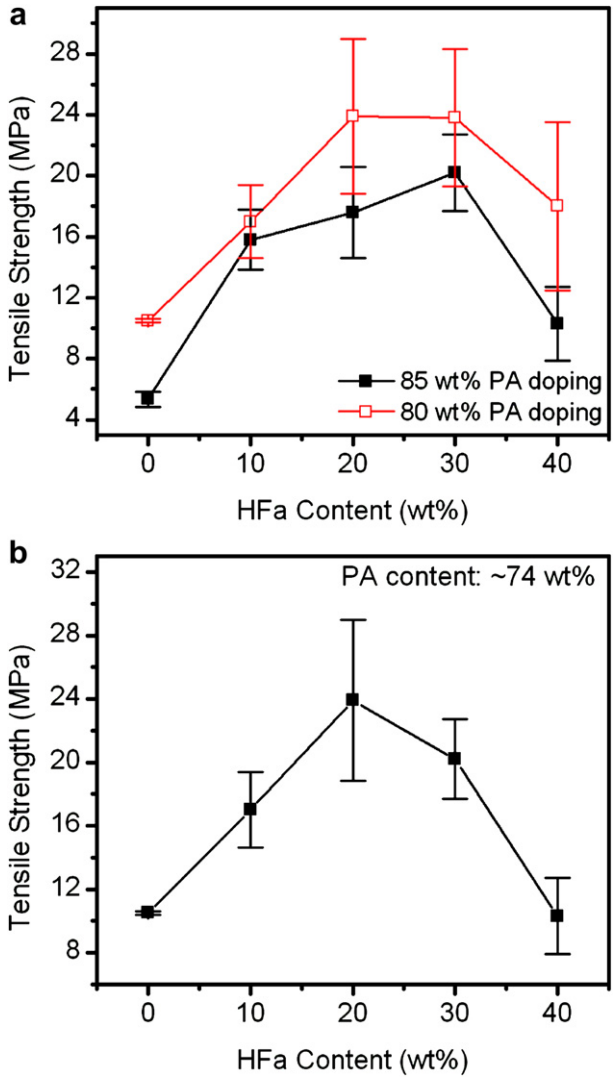

Fig. 6. Tensile strength of P(HFa-*co*-BI) membranes with HFa contents a) after immersion in 80 wt.% (open) and 85 wt.% (closed) and b) at 74 wt.% of PA content.

use in fuel cell applications at elevated temperatures. Meanwhile, the decrease in tensile strength values of P(HFa-*co*-BI) membranes with a large amount of HFa up to 40 wt.% is mainly attributed to poly(benzoxazine)s, since it is brittle by nature [40]. Similar decreases in the mechanical properties were observed in the cross-linked copolymer membranes prepared from mono-functional benzoxazines when the benzoxazine contents were larger than a certain amount depending on the benzoxazine structures [19,20].

A critical issue in state-of-the-art PEM studies is the electrochemical lifetime during operation. The durability of PEMs was assessed by the *in situ* acceleration lifetime test (ALT), which has been regarded as a credible and time-saving method to effectively predict PEM lifetime under real fuel cell operating conditions over time [43–45]. In this study, the severe operating conditions of the dynamic mode (load changing test cycle) were employed to age cells after completely establishing the cells under stationary conditions. The drop in open circuit voltage (OCV) below 0.9 V implies evolution on the microstructure of the membrane and was considered as an ALT screening criterion that occurs before failure of the membranes caused by mechanical damage such as membrane thinning and pin-hole formation [43,46]. On the basis of mechanical and electrical properties, the P(HFa-*co*-BI)-30 membrane was chosen to compare the durability with PBI

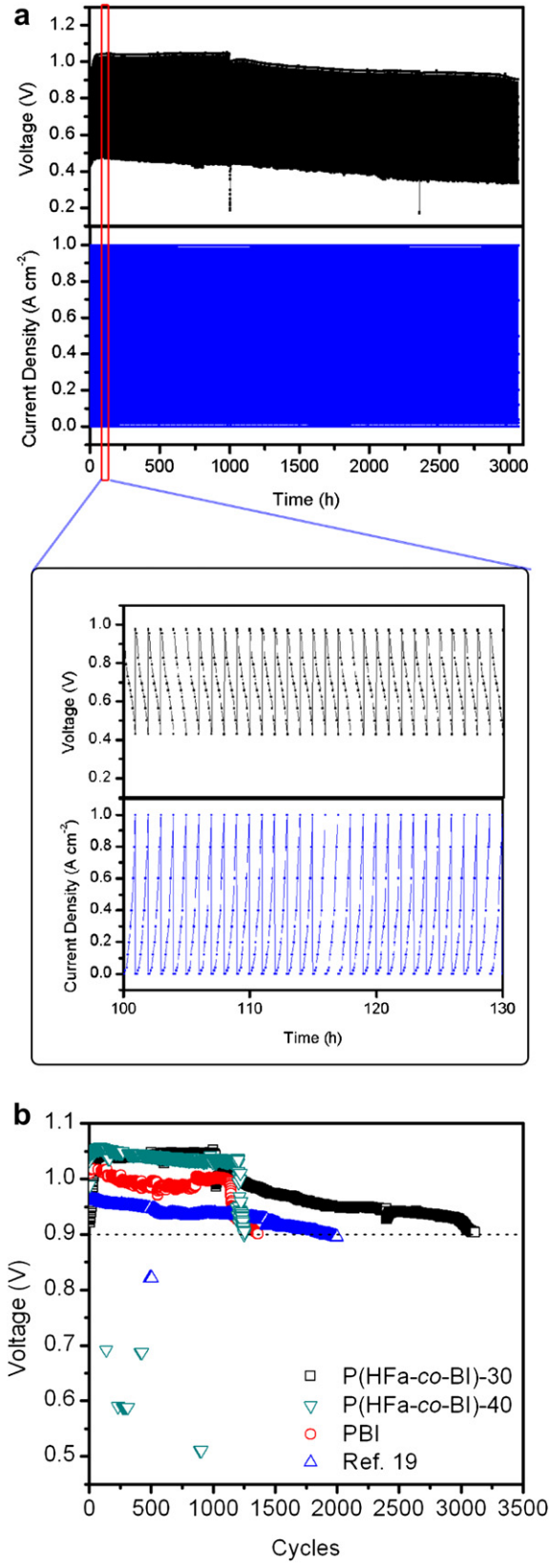

Fig. 7. a) *In situ* acceleration lifetime test (load changing test cycle) of P(HFa-*co*-BI)-30 membranes at 150 °C, non-humidified H_2 and air (ambient pressure), cathode; 0.9 mg cm^{-2} PtRu loading, anode; 1.7 mg cm^{-2} PtCo loading. Active area is 7.84 cm^2. b) The variations in OCV of P(HFa-*co*-BI)-30, P(HFa-*co*-BI)-40, PBI, and cross-linked benzoxazine-benzimidazole copolymer membrane prepared by mono-functional benzoxazine (from Ref. [19]) as a function of cycles on *in situ* ALT mode.

membrane. The P(HFa-*co*-BI)-30 membrane endured over 3066 h of ALT at 150 °C (Fig. 7). Its number of load cycles is approximately 3116, whereas that of the PBI membrane is only 1360. The lifetime loss of the P(HFa-*co*-BI)-30 membrane during ALT was calculated from the variation in OCV with run time, which was found to have a rate of −0.04 mV h^{-1} until failure at 3066 h [47]. In contrast, the lifetime loss of the P(HFa-*co*-BI)-40 and PBI membranes increases quickly at a rate of −0.11 and −0.08 mV h^{-1}, respectively, which led to rapid failure within 1360 h. The longest lifetime of previous cross-linked benzoxazine-benzimidazole copolymers on *in situ* ALT was 2000 h (1999 cycles) with −0.03 mV h^{-1} of lifetime loss [19]. The long-term durability of P(HFa-*co*-BI)-30 membrane could be ascribed to the improved mechanical and thermooxidative stabilities of the material having cross-linked structures formed by the di-functional benzoxazine. For instance, the tensile strength of P(HFa-*co*-BI)-30 membrane is larger by 50% than those of P(HFa-*co*-BI)-40 and PBI membranes at the same PA content (Fig. 6) and all of P(HFa-*co*-BI) membranes are more thermally stable than PBI membrane (Fig. S3 in Supplementary data). Besides, it was also well-known that the *I*–*V* curves can drop rapidly within a short period of time when the compatibility of electrode layers and the membranes is not good [48,49]. Therefore the increase in compatibility between the P(HFa-*co*-BI) membranes and the electrode prepared with PVDF binder materials (they both have fluorinated moieties) improve the cell performance and can also contribute to the increase of long-term durability of the MEAs.

4. Conclusions

Cross-linked copolymer, P(HFa-*co*-BI), membranes are prepared using di-functional benzoxazine (HFa) and PBI by a solution casting method with subsequent stepwise heating and even large-sized films could be easily prepared by a slot die coating technique, enabling the growth of production. The proton conductivity values of P(HFa-*co*-BI) membranes are found to be smaller than that of PBI membrane when they have similar PA contents, which is mostly due to the cross-linked structures of P(HFa-*co*-BI)s. Their cell performances, however, are comparable with that of PBI membrane due to the decrease of the interfacial resistance of membranes with electrodes. The membrane and electrode materials both have fluorinated moieties, which could increase their compatibility. In particular, the long-term durability (*ca.* 3116 cycles on *in situ* ALT mode), one of the most important properties for the application of polymer membranes in PEMFCs, is 2- and 1.5-times longer for the P(HFa-*co*-BI)-30 membrane than for the PBI and cross-linked copolymers prepared from mono-functional benzoxazine, respectively, on *in situ* ALT mode.

Acknowledgments

This research was supported by Samsung Advanced Institute of Technology, Samsung Electronics Co., Ltd. through the Brain Korea Program and the Fundamental R&D Program of World Premier Materials (WPM) funded by the Ministry of Knowledge Economy, Republic of Korea.

Appendix A. Supplementary data

Supplementary data related to this article can be found at http://dx.doi.org/10.1016/j.jpowsour.2012.11.019.

References

[1] Q. Li, R. He, J.O. Jensen, N.J. Bjerrum, Chem. Mater. 15 (2003) 4896–4915.
[2] J. Zhang, Z. Xie, J. Zhang, Y. Tang, C. Song, T. Navessin, Z. Shi, D. Song, H. Wang, D.P. Wilkinson, Z.-S. Liu, S. Holdcroft, J. Power Sources 160 (2006) 872–891.
[3] H.K. Kim, D.H. Kim, J. Choi, S.C. Kim, Macromol. Res. 19 (2011) 928–942.
[4] J.-M. Song, J. Shin, J.-Y. Sohn, Y.C. Nho, Macromol. Res. 19 (2011) 1082–1089.
[5] J.A. Hurd, R. Vaidhyanathan, V. Thangadurai, C.I. Ratcliffe, I.L. Moudrakovski, G.K.H. Shimizu, Nat. Chem. 1 (2009) 705–710.
[6] Y. Shao, G. Yin, Z. Wang, Y. Gao, J. Power Sources 167 (2007) 235–242.
[7] W. Ma, C. Zhao, J. Yang, J. Ni, S. Wang, N. Zhang, H. Lin, J. Wang, G. Zhang, Q. Li, H. Na, Energy Environ. Sci. 5 (2012) 7617–7625.
[8] J. Weber, K.-D. Kreuer, J. Maier, A. Thomas, Adv. Mater. 20 (2008) 2595–2598.
[9] Q. Li, R. He, J.O. Jenson, N.J. Bjerrum, Fuel Cells 4 (2004) 147–159.
[10] J. Lobato, P. Cañizares, M.A. Rodrigo, J.J. Linares, G. Manjavacas, J. Membr. Sci. 280 (2006) 351–362.
[11] D. Weng, J.S. Wainright, U. Landau, R.F. Savinell, J. Electrochem. Soc. 143 (1996) 1260–1263.
[12] Q. Li, J.O. Jensen, R.F. Savinell, N.J. Bjerrum, Prog. Polym. Sci. 34 (2009) 449–477.
[13] J. Mader, L. Xiao, T.J. Schmidt, B.C. Benicewicz, Adv. Polym. Sci. 216 (2008) 63–124.
[14] E. Quartarone, P. Mustarelli, Energy Environ. Sci. 5 (2012) 6436–6444.
[15] Q. Li, C. Pan, J.O. Jensen, P. Noyé, N.J. Bjerrum, Chem. Mater. 19 (2007) 350–352.
[16] J. Kerres, A. Ullrich, F. Meier, T. Häring, Solid State Ionics 125 (1999) 243–249.
[17] H.-S. Lee, A. Roy, O. Lane, J.E. McGrath, Polymer 49 (2008) 5387–5396.
[18] K. Miyatake, T. Tombe, Y. Chikashige, H. Uchida, M. Watanabe, Angew. Chem. Int. Ed. 46 (2007) 6646–6649.
[19] S.-K. Kim, S.-W. Choi, W.S. Jeon, J.O. Park, T. Ko, H. Chang, J.-C. Lee, Macromolecules 45 (2012) 1438–1446.
[20] S.-K. Kim, T. Ko, S.-W. Choi, J.O. Park, K.-H. Kim, C. Pak, H. Chang, J.-C. Lee, J. Mater. Chem. 22 (2012) 7194–7205.
[21] T.-H. Kim, T.-W. Lim, J.-C. Lee, J. Power Sources 172 (2007) 172–179.
[22] M.-H. Jeong, K.-S. Lee, J.-S. Lee, Macromolecules 42 (2009) 1652–1658.
[23] Y.-X. Wang, H. Ishida, Polymer 40 (1999) 4563–4570.
[24] T. Steenberg, H.A. Hjuler, C. Terkelsen, María T.R. Sánchez, L.N. Cleemann, F.C. Krebs, Energy Environ. Sci. 5 (2012) 6076–6080.
[25] J. Höpken, M. Möller, Macromolecules 25 (1992) 1461–1467.
[26] R. Bouchet, E. Siebert, Solid State Ionics 118 (1999) 287–299.
[27] A. Bozkurt, W.H. Meyer, G. Wegner, J. Power Sources 123 (2003) 126–131.
[28] C.H. Lee, S.Y. Lee, Y.M. Lee, S.Y. Lee, J.W. Rhim, O. Lane, J.E. McGrath, ACS Appl. Mater. Interfaces 1 (2009) 1113–1121.
[29] Y.S. Kim, M.J. Sumner, W.L. Harrison, J.S. Riffle, J.E. McGrath, B.S. Pivovar, J. Electrochem. Soc. 151 (2004) A2150–A2156.
[30] K.B. Wiles, C.M. de Diego, J. de Abajo, J.E. McGrath, J. Membr. Sci. 294 (2007) 22–29.
[31] A.G. Hombrados, L. González, M.A. Rubio, W. Agila, E. Villanueva, D. Guinea, E. Chinarro, B. Moreno, J.R. Jurado, J. Power Sources 151 (2005) 25–31.
[32] S.-J. Seo, J.-J. Woo, S.-H. Yun, H.-J. Lee, J.-S. Park, T. Xu, T.-H. Yang, J. Lee, S.-H. Moon, Phys. Chem. Chem. Phys. 12 (2010) 15291–15300.
[33] O. Himanen, T. Hottinen, M. Mikkola, V. Saarinen, Electrochim. Acta 52 (2006) 206–214.
[34] X. Yuan, H. Wang, J.C. Sun, J. Zhang, Int. J. Hydrogen Energy 32 (2007) 4365–4380.
[35] B.G. Choi, J. Hong, W.H. Hong, P.T. Hammond, H.S. Park, ACS Nano 5 (2011) 7205–7213.
[36] D.R. Lawson, L.D. Whiteley, C.R. Martin, M.N. Szentirmay, J.I. Song, J. Electrochem. Soc. 135 (1988) 2247–2253.
[37] S. Gottesfeld, I.D. Raistrick, S. Srinivasan, J. Electrochem. Soc. 134 (1987) 1455–1462.
[38] Z. Ogumi, T. Kuroe, Z.-I. Takehara, J. Electrochem. Soc. 132 (1985) 2601–2605.
[39] S.S. Hosseini, M.M. Teoh, T.S. Chung, Polymer 49 (2008) 1594–1603.
[40] R. He, Q. Li, A. Bach, J.O. Jensen, N.J. Bjerrum, J. Membr. Sci. 277 (2006) 38–45.
[41] N.N. Ghosh, B. Kiskan, Y. Yagci, Prog. Polym. Sci. 32 (2007) 1344–1391.
[42] T. Agag, T. Takeichi, Macromolecules 34 (2001) 7257–7263.
[43] M. Marrony, R. Barrera, S. Quenet, S. Ginocchio, L. Montelatici, A. Aslanides, J. Power Sources 182 (2008) 469–475.
[44] S. Zhang, X. Yuan, H. Wang, W. Mérida, H. Zhu, J. Shen, S. Wu, J. Zhang, Int. J. Hydrogen Energy 34 (2009) 388–404.
[45] P. Pei, Q. Chang, T. Tang, Int. J. Hydrogen Energy 33 (2008) 3829–3836.
[46] V.O. Mittal, H.R. Kunz, J.M. Fenton, J. Electrochem. Soc. 153 (2006) A1755–A1759.
[47] S. Yu, L. Xiao, B.C. Benicewicz, Fuel Cells 8 (2008) 165–174.
[48] M. Sankir, Y.S. Kim, B.S. Pivovar, J.E. McGrath, J. Membr. Sci. 299 (2007) 8–18.
[49] C.H. Lee, S.Y. Lee, Y.M. Lee, J.E. McGrath, Langmuir 25 (2009) 8217–8225.